Accepted Manuscript

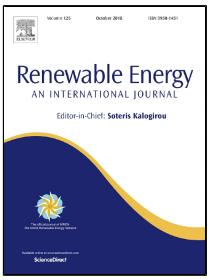

High temperature corrosion behaviour on molten nitrate salt-based nanofluids for CSP plants

Angel G. Fernández, Belen Muñoz-Sánchez, Javier Nieto-Maestre, Ana García-Romero

PII:	S0960-1481(18)30803-6
DOI:	10.1016/j.renene.2018.07.018
Reference:	RENE 10292
To appear in:	*Renewable Energy*
Received Date:	08 February 2018
Accepted Date:	03 July 2018

Please cite this article as: Angel G. Fernández, Belen Muñoz-Sánchez, Javier Nieto-Maestre, Ana García-Romero, High temperature corrosion behaviour on molten nitrate salt-based nanofluids for CSP plants, *Renewable Energy* (2018), doi: 10.1016/j.renene.2018.07.018

High temperature corrosion behaviour on molten nitrate salt-based nanofluids for CSP plants

Angel G. Fernández[1*], Belen Muñoz-Sánchez[2,3], Javier Nieto-Maestre[3], Ana García-Romero[2]

[1]Energy Development Center. University of Antofagasta. Avenida Universidad de Antofagasta 02800, Antofagasta, Chile.

[2]Department of Mining Engineering, Metallurgy and Materials Science, University of the Basque Country (UPV/EHU), Rafael Moreno "Pitxitxi", 2. 48013 - Bilbao (Vizcaya). Spain.

[3]Tecnalia Research and Innovation, Mikeletegi Pasealekua, 2. 20009 - San Sebastián (Guipúzcoa). Spain.

*Corresponding author E-Mail: angel.fernandez@uantof.cl

Abstract

Recently, a number of theoretical and experimental studies have been performed to understand the effect of nanoparticles on thermal properties and heat transfer performance but there is a lack regarding their corrosion properties. In this work, an extended corrosion characterization (at central tower plant storage temperature (565ºC)) has been carried out in two different grades of solar salt (industrial and refined purity) doped with the addition of 1 wt% Al_2O_3 nanoparticles or 1 wt% SiO_2 nanoparticles. Corrosion rates were determined in commercial stainless steel commonly used in CSP technology (347SS) by gravimetric tests, measuring the weight gain during 1000 hours, identifying the corrosion products by Scanning Electron Microscopy (SEM) and X-Ray Diffraction (XRD). The lowest corrosion rate (0.007 mm/year) was obtained in the refined solar salt with the addition of 1 wt% Al_2O_3 nanoparticles. A protective layer was formed in the steel-salt interphase, identified through XRD as Al_2O_3.

Additionally, hematite (Fe_2O_3) and magnetite (Fe_3O_4) were obtained as unprotective corrosion products throughout the test carried out with or without nanoparticles. In addition, the presence of impurities on the salts generated some stable compounds, as magnesium ferrite ($MgFe_2O_4$).

Keywords: Nanoparticles; molten salts; corrosion; Concentrated Solar Power

List of nomenclatures:

CSP: Concentrated Solar Power
SEM: Scanning Electron Microscopy
XRD: X-ray diffraction
TES: Thermal Energy Storage
LCOE: Levelized Cost of Electricity
RSS: Refined Solar Salt
ISS: Industrial Solar Salt
ANP: Alumina Nanoparticle
SiNP: Silica Nanoparticle
EDX: Energy Dispersive X-**Ray**

1. Introduction

Concentrating Solar Power (CSP) technology captures and stores the sun's energy in the form of heat, using materials that are low cost and stable for decades. Today's most advanced CSP systems are towers integrated with two-tank molten-salt TES, delivering thermal energy at 565 °C for integration with conventional steam-Rankine power cycles [1]. This design has lowered the cost of CSP electricity by approximately 50% over the prior generation of parabolic trough systems. However, the decrease in cost of CSP technologies has not kept pace with the falling cost of solar photovoltaic systems and further research is needed. High-temperature molten salt has been commonly used as an effective working fluid for CSP systems, increasing electrical efficiency and reducing the Levelized Cost of Electricity (LCOE). However, the high freezing point of the Solar Salt (221 ºC) may result in its solidification on a cloudy day or at night. In this direction, the design of multicomponent mixtures by the addition of alkali/alkaline earth nitrates could extend the working temperature range of thermal energy storage [2, 3] but an enhancement in the thermal conductivity and heat capacity at storage temperatures must be necessary for a successful development of this technology.

In this direction, high temperature nanofluids have received great attention over the last decade due to their increased specific heat compared to the base fluids [4, 5]. In the last years, several researches have been performed to understand the effect of nanoparticles on thermal properties and heat transfer performance [6-10]. These researches have been focused on Thermal Energy Storage (TES) materials (molten salts) commonly used in

Concentrated Solar Power (CSP) plants and a majority of the works [10-12] showed that the specific heat of nano-salt was increased. The percentage of addition (used in this work, 1wt.%) is based on the excellent thermal transfer obtained by several authors with the same nanofluids [5]. Many efforts have been required to carry out the research work published up to date due to the lack of standards for the preparation, the measurement and the evaluation of the results, as well as to approach the understanding of the behaviour of the composite at the nano-scale [13]. Therefore, the fact of having the nanoparticles well-dispersed rather than agglomerated is one of the objective in this technology since it will cause fluidity issues or higher corrosion behavior. Well-dispersed nanoparticles essentially result in an increased surface to volume ratio, which can lead to enhanced thermal conductivity, a transport-related property. Jo et al.[4] conclude that a compressed liquid creates a layer adjacent to the interface with the solid and the specific heat capacity enhancement in a nanomaterial can result from an increased interface area between the surrounding liquid and the nanoparticles improving the specific heat capacity of nanomaterials.

Different authors [14-17] have evaluated the effect of the impurities in the convencional molten salts proposed as thermal energy storage material concluding that impurities tend to drive corrosion. However, there is not information in the literature regarding the corrosive effect in molten salt based nanofluids. The corrosive evaluation of these improved molten salts must be studied since nanoparticles are solid in the mixture, being potential candidates to promote erosion/corrosion in CSP pipelines.

This is one of the main factors to take into account in the corrosion test performed during 1000 hours. The aim of this paper is the corrosive evaluation of two grades of solar salt (SQM, Refined (RSS) and Industrial (ISS) grades) with the most common addition of Al_2O_3 and SiO_2 nanoparticles found in the literature (1wt.%), at 565 ºC in contact with 347SS.

2. Materials and methods

The saline nitrates used in the research were $NaNO_3$ and KNO_3 (SQM grades RSS and ISS). Two Solar Salts (60:40 wt. of $NaNO_3$:KNO_3) of different purity were prepared: the refined grade, RSS (SQM, $NaNO_3$≥99.5 wt.%; SQM, KNO_3≥99.6 wt.%) and the industrial grade, ISS (SQM, $NaNO_3$≥98.0 wt.%; SQM, KNO_3≥95.0 wt.%). Two types of ceramic nanoparticles were selected, Al_2O_3 nanoparticles

(ANPs) and SiO_2 nanoparticles (SiNPs). ANPs were purchased from Kawaken Chemicals as an industrial water-based nanofluid, Alumisol 10A, containing fiber-shaped boehmite nanoparticles (L=50 nm, ϕ=10 nm) at 10 wt% according to the manufacturer. The boehmite (aluminium oxyhydroxide, AlOOH) is a precursor of the γ-Al_2O_3. On the other side, a dispersion of colloidal silica at 30 wt%, Ludox SM-30, from Sigma-Aldrich was used as a source of spherical SiNPs.

Four nanofluids were produced with these materials, including 1 wt.% of each nanoparticle in combination with each of the salts RSS and ISS. Once the synthesis process involving nanoparticles addition was arranged (addition procedure was explained in a previous paper [18]), the mixed formulations were sealed inside a dry box with desiccants. The steel analyzed in the saline medium was an austenitic stainless steel (347SS, 2%Mn/11%Ni/18%Cr) commonly proposed as container material in CSP plants.

The dimensions of the steel samples used in the gravimetric corrosion tests were 20 mm × 10 mm × 2 mm. A grinding process was performed using silicon carbide (SiC) P1000 abrasive paper with a (SiC grit size: 18.3 μm). This treatment produces a homogeneous surface in the sample and promotes delamination of the possible oxides and the small imperfections where corrosion could be located. The samples were subsequently washed with acetone in an ultrasound bath to eliminate any remaining dirt. The dimensions of each sample were measured using an electronic caliber (± 0.01mg), and each sample was weighed using an analytical balance (Mettler Toledo) with a 0.00001 g responsiveness. Subsequently, the samples were placed into alumina crucibles (Fig 1) with the saline mixture and then heated in a resistance furnace at 565 °C.

Figure 1. Alumina crucibles filled in with nanofluid (left) and alloy specimen immersed into the solid nanodoped-salt before the test (right).

Table 1: Impurity content in solar salts employed in this work

Impurity	RSS Solar Salt (wt%)	ISS Solar Salt (wt%)
Chloride	0.060	0.260
Perchlorate	0.064	0.247
Sulfate	0.011	0.146
Carbonate	0.010	0.009
Nitrite	<0.001	<0.001

Different technical grades of solar salt (refined and industrial) have been selected for the nanoparticles addition since the impurities present in the salt could have influence in the integration of these particles in the salt matrix. Static gravimetric measurements were performed after 200, 400, 600, 800 and 1000 hours of exposure at the testing temperature in the isothermal immersion test. After the samples were removed from the crucible, they were left to cool down slowly and subsequently washed out with warm distilled water to eliminate the salt in which they were immersed and they were dried and weighed. Five weight measurements were taken from each sample and between each measurement the samples were kept into dry box with desiccants. The average value of the weight obtained from the five measurements has been used for the analysis of the results. The formula (Eq. 1) to calculate the mass gain over time is:

$$\frac{\Delta \mathrm{m}}{S_0} = \frac{m_f - m_i}{S_0} \qquad \text{(Eq 1)}$$

where m_i is the initial mass of the specimen, m_f is the mass of the same at time t and S_0 is the initial area of the specimen. Finally, the microstructural characterization has been carried out in a scanning electron microsopy (SEM, JEOL 6460LV with EDAX)), using EDS analysis in order to stablish the morphology as well as the corrosion mechanism. X-ray diffraction analysis (with a grazing angle of 0.5º) model X'Pert Pro/MRD from Panalytical was used for the corrosion components elucidation after 1000 hours of test.

3. Results

3.1. Corrosion of ISS and its nanofluids

The gravimetric weight gain that occurs on ISS is shown in figure 2, where the results obtained with the industrial grade solar salt (ISS) and its corresponding nanofluids (the ISS with 1%Al_2O_3, and the ISS with 1%SiO_2) can be compared.

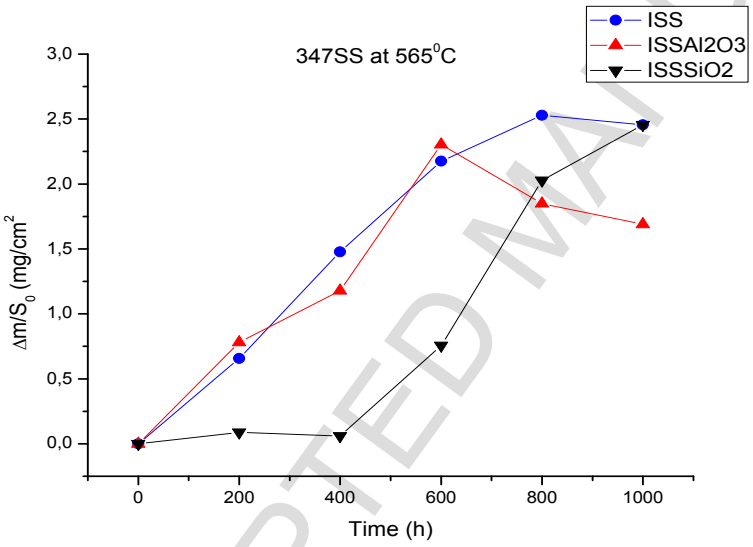

Figure 2: Gravimetric weight gain curve obtained in ISS and its nanofluids for 347SS at 565ºC

At 600 hours of experiment, the corrosion produced by ISS + 1% Al_2O_3 was higher compared with the weight gain in the solar salt without nanoparticles. Beyond this point the corrosion rate is reduced, probably due to the sedimentation of the nanoparticles at the bottom of the crucible.

To explain this behavior, a micro-structural (surface and cross section) study of the SS347 was performed using scanning electron microscopy (SEM). Figure 3 shows the sample surface morphology of the steel after 800 hours of exposure to ISS + 1 %wt. Al_2O_3, as well as an analysis via Energy-Dispersive X-ray spectroscopy (EDX) of the particles

found on the surface. At the end of the test, a uniform sodium ferrite (Na_2FeO_4) scale was obtained.

Spectrum	O	Na	Fe
Spectrum 1	40.28	32.59	27.13
Spectrum 2	38.99	20.21	40.80

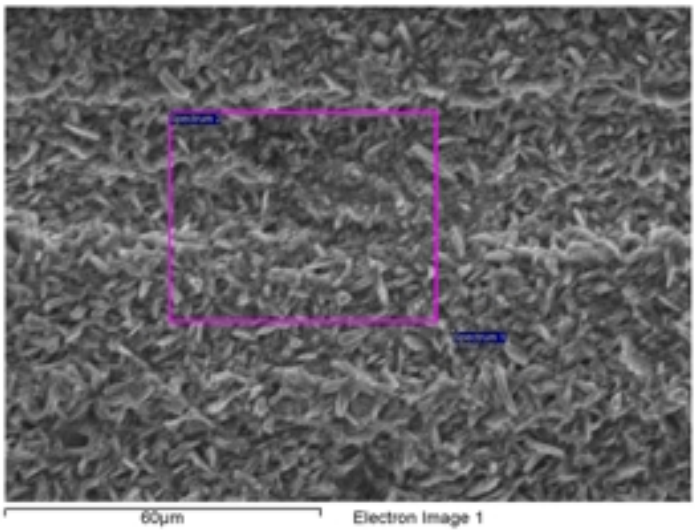

Figure 3: Detail of the 347SS specimen surface after 800 hours immersed into ISS+1%Al_2O_3

For the cross sectional study, SEM pictures have been obtained by backscattered electron microscopy.

Spectrum	*O*	*Na*	*Si*	*K*	*Ca*	*Cr*	*Mn*	*Fe*	*Ni*
Spectrum 1	38.58	7.39	-	-	0.26	0.77	1.36	51.64	-
Spectrum 2	33.20	1.24	-	0.23	-	2.05	1.42	61.40	0.47
Spectrum 3	28.72	1.49	0.80	0.26	-	4.40	1.71	61.74	0.88
Spectrum 4	19.85	0.72	1.02	-	-	28.00	1.59	38.64	10.19
Spectrum 5	14.83		0.71	-	-	20.06	1.35	46.82	16.23

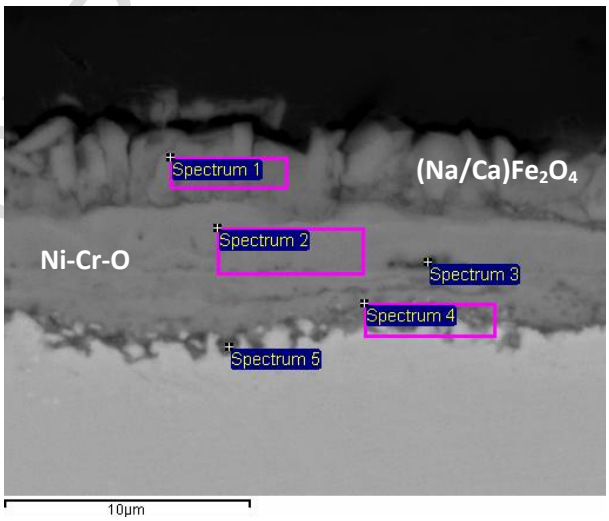

Figure 4: Detail of the cross-section of the 347SS specimen after 1000 hours immersed into ISS+1%Al_2O_3

A protective layer composed by Ni-Cr-O has been detected in the steel surface and in the upper part an non protective layer composed by (Na/Ca)Fe_2O_4 was obtained, trough the following reactions:

$$Na_2O + Fe_2O_3 \rightarrow Na_2Fe_2O_4 \qquad \text{(Reac. 1)}$$

$$CaO + Fe_2O_3 \rightarrow CaFe_2O_4 \qquad \text{(React. 2)}$$

On the other hand, for ISS+1 wt.%SiO_2, the analysis of the surface shown in figure 5 presents a less compact corrosion layer, probably due to the Si content detected in the corrosion layer. This influence of the Si presence in corrosion layers was recently publish by Hamid et al. [19], concluding that 1 wt% Si additions could modify the steel surface interacting with the impurities present in the corrosive environment along with the alloying elements of the steel.

Spectrum	*O*	*Na*	*Mg*	*Si*	*Ca*
Spectrum 1	64.69	35.31	-	-	-
Spectrum 2	64.29	8.15	-	-	27.56
Spectrum 3	45.89	27.72	9.12	17.27	-

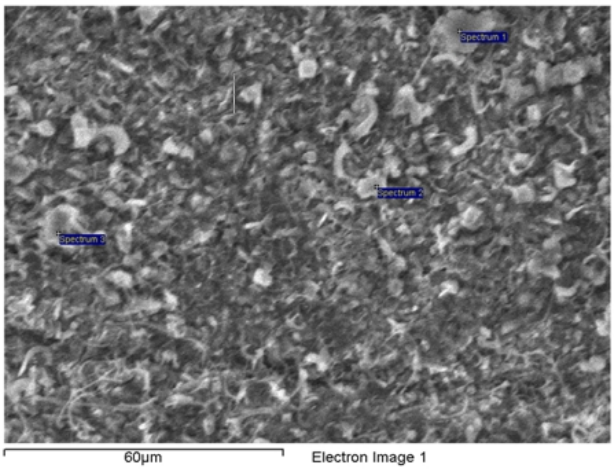

Figure 5: Superficial image of 347SS immersed during 800 hours in ISS+1 wt.% SiO_2

This silicon content was also detected in the cross sectional study at different levels through the corrosion layer. The composition of these products have been determined by XRD (table 2) and in this case, SiO_2 and Fe_2SiO_4 were identified in the steel and in the remaining salt after the corrosion test.

Spectrum	O	Na	Mg	Si	K	Ca	Cr	Mn	Fe	Ni
Spectrum 1	50.96					47.81			1.23	
Spectrum 2	32.71	0.94	0.41	0.42			8.27	1.62	52.67	2.96
Spectrum 3	35.32	2.08	1.61	0.42		7.45	3.50	1.52	36.80	11.29
Spectrum 4	35.15	4.66	3.54		0.34		0.59	1.02	54.70	
Spectrum 5	18.45		0.84	0.67		0.29	16.75	1.80	52.55	8.65
Spectrum 6				0.42			13.90	1.14	72.62	11.91

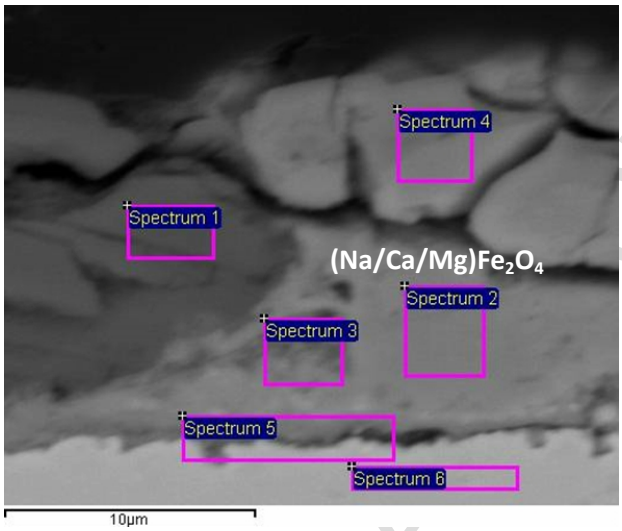

Figure 6: Cross sectional image of 347SS immersed during 1000 hours in ISS+1 wt.%SiO_2.

A non protective layer composed by (Na-Ca-Mg)Fe_2O_4 has been formed in the corrosion layer, responsible of the higher gravimetric weight gain determined when the steel is immersed into ISS+1 wt.%SiO_2 as shown in figure 1.

It is important to highlight that the stability of the salts during the corrosion process showed an important reduction when SiO_2 nanoparticles are involved and the salt solidified two times during the corrosion test.

Yang et al. [20] reported that when molten nitrate salts come into contact with a containment substrate such as quartz or stainless steel at temperatures above 500ºC, the release of nitrogen oxide could be foreseen due to the extensive reaction of NO_3^- with SiO_2 or with Cr, respectively. The reactions included:

$$SiO_2 + 2NO_3^- \leftrightarrow SiO_4^{2-} + 2NO_2 \quad \text{(Reac. 3)}$$

$$\text{and } Cr + 2NO_3 \leftrightarrow CrO_4^{2-} + 2NO \quad \text{(Reac. 4)}$$

The results attained in our work revealed that the presence of the SiO_2 nanoparticles promotes the decomposition of nitrate or nitrite to form silicates (Na_2SiO_3) and NO gas.

3.2. Corrosion of RSS and its nanofluids

In order to compare the corrosion behavior produced by a Solar Salt with a different impurity content (lower percentage of chloride), RSS provided by SQM has been studied. In this case, the gravimetric weight gain is lower compared to the previous case using ISS and there is not a clear correlation between the corrosion produced by the addition of nanoparticles to the RSS. The better corrosion behavior was obtained for RSS+1 wt.%Al_2O_3 showing a gravimetric weight gain around 0.5 mg/cm^2.

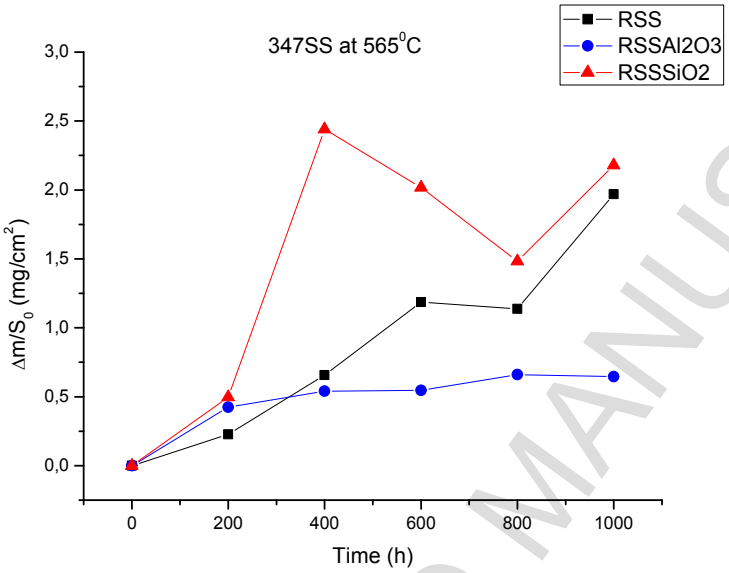

Figure 7: Gravimetric weight gain of the 347SS specimens immersed into the refined solar salt (RSS) and the corresponding nanofluids at 565ºC

In this direction, it is important to highlight the morphology of the specimens surface immersed in RSS+1 wt.%Al_2O_3 (figure 7), showing needle-like structures containing Al. This structure, integrated in the steel matrix, increase the protection against the corrosion produced by molten salts.

261

Spectrum	*C*	*O*	*Na*	*Mg*	*Ca*	*Cr*	*Mn*	*Fe*
Spectrum 1	12.84	40.40	5.98	1.73	4.49	1.14	0.89	32.53
Spectrum 2	9.89	33.31	9.59	1.59	3.07	1.13	3.34	38.09
Spectrum 3	7.99	36.09	4.93	2.85	4.80	1.18	2.08	40.08

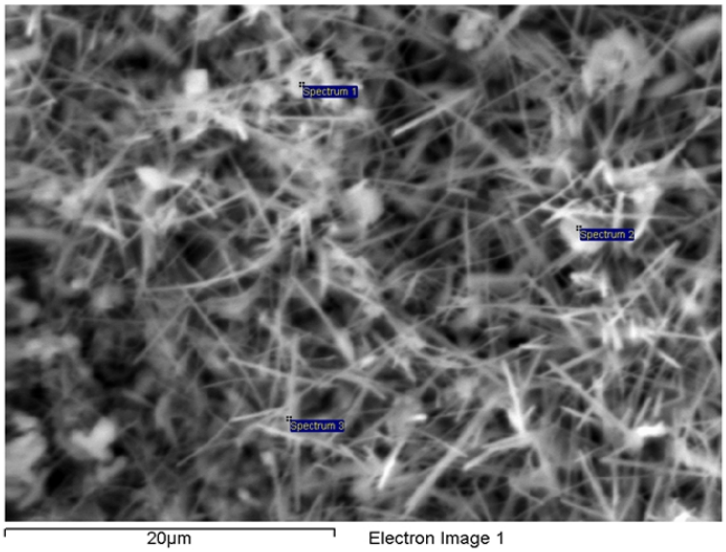

262

263 Figure 8: Detail of the surface morphology of a 347SS specimen immersed in RSS+1 wt.%Al_2O_3
264 for 800 hours.

265 Presently, there is no a clear explanation about the potential mechanism leading to the
266 corrosion protection obtained by this needle-like aluminium oxide morphology.
267 An extended research will be carried out in the future to understand the fundamentals
268 behind the better corrosion behaviour due to the Al_2O_3 nanoparticles. On the other hand,
269 the formation of this corrosion-protective layer could reduce the heat capacity
270 enhancement produced in the molten salt by the addition of the nanoparticles, which was
271 indeed the main objective pursued in their development [11, 18]. If a synergic effect
272 between the corrosion protection and the thermal properties could be attained, the key for
273 an interesting increment of the efficiency and the cost reduction of this technology could
274 have been found.
275 The alumina needles were also observed on the cross sections of the specimens, like that
276 shown in figure 8. In this case a compact protective layer of spinel ($FeCr_2O_4$) formed on
277 the steel surface, which leads to increase the corrosion resistance of the steel in contact
278 with the molten salt.

279

280

Spectrum	*O*	*Na*	*Mg*	*Al*	*Si*	*Cl*	*K*	*Ca*	*Cr*	*Mn*	*Fe*	*Ni*
Spectrum 1	32.35	0.75	0.48					0.84	10.99	1.83	50.68	2.09
Spectrum 2	36.13	7.28	1.41	0.76		0.32		1.05	0.98	1.70	50.38	
Spectrum 3	32.76	0.59	0.58		0.37			0.54	11.16	1.96	51.48	0.55
Spectrum 4	29.06				0.81		0.36		29.69	2.22	34.50	3.36

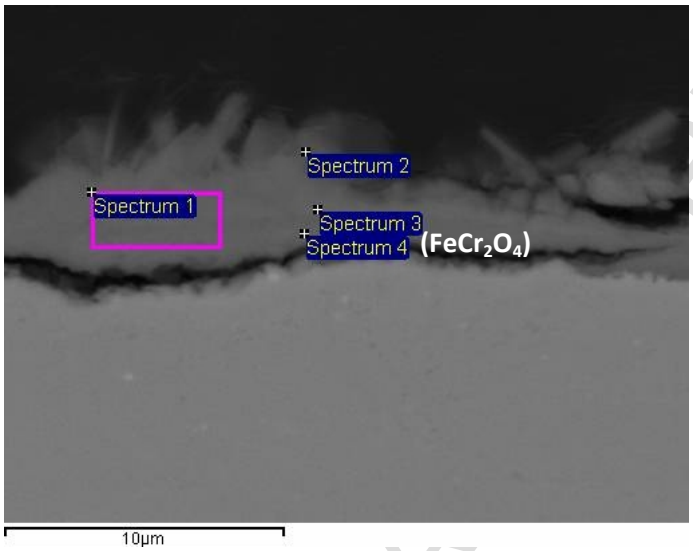

Figure 9: Detail of the 347SS specimen cross-section immersed into ISS+1%Al_2O_3 for 1000 hours

According to the obtained gravimetric curve (figure 7), the steel immersed in the refined solar salt containing 1 wt.%SiO_2, presents irregularities on the mass increment. This behavior could be explained due to the spallation of the oxidic layer, as can be observed on the surface morphology of the specimen shown in figure 10.

Spectrum	*O*	*Na*	*K*	*Ca*	*Cr*	*Fe*
Spectrum 1	30.71	13.78	-	-	4.74	50.76
Spectrum 2	34.34	24.77	0.79	2.24	-	37.86

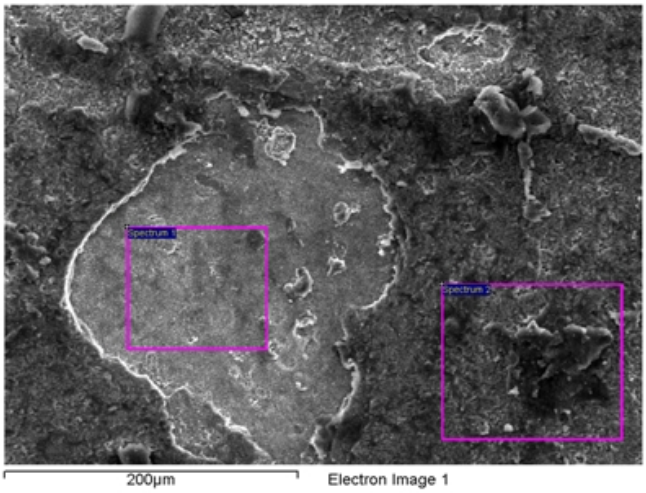

Figure 10: Detail of the 347SS specimen surface after immersed in RSS+1 wt.%SiO_2 for 800 hours

The EDX analysis of the surface after the oxide-spallation was carried out (pink box on the left, in figure 10), as well as the analysis of the oxide surface adhered to the specimen (pink box on the right, in figure 10). The composition of the surface after spallation (spectrum 1) presents a higher Cr content.

This is a protective layer, which was seen in the cross section of the specimen (figure 11) in the inner zone, close to the steel surface. In this case the thickness of the corrosion layer obtained was 12.13 microns at the end of the test, showing the higher weight gain according the gravimetric curve (figure 7).

Spectrum	*O*	*Na*	*Si*	*Cr*	*Mn*	*Fe*	*Ni*
Spectrum 1	35.50	7.07	0.57	0.96	0.86	55.05	-
Spectrum 2	29.12	-	0.56	6.15	1.28	59.22	3.66
Spectrum 3	19.78	-	0.68	30.35	1.74	31.07	16.37
Spectrum 4	32.24	-	1.14	14.90	1.99	47.12	2.61
Spectrum 5	17.70	-	0.71	28.50		35.72	17.37

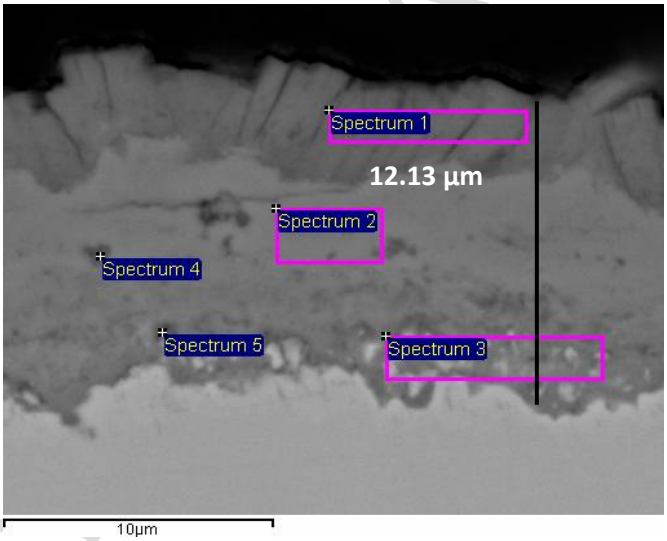

Figure 11: Detail of the 347SS specimen cross-section after immersed into ISS+1 wt.%SiO_2 for 1000 hours

XRD analysis were carried out after the corrosion test, both in the samples as well as in the salts in contact with them. Results are shown in table 2.

340 Table 2: Corrosion products obtained by XRD in the steels tested and in the salt remaining

Molten salts	Nano particle	Steel	Corrosion products		Corrosion rate (mm/year)
			Steel	Salt	
Solar Salt RSS Grade	Al_2O_3 (1 wt%)	347	$MgFe_2O_4$, Fe_2O_3, Fe_3O_4, Al_2O_3	$K_2Fe_2O_4$	0.007
	SiO_2 (1 wt%)	347	Fe_3O_4, Fe_2O_3, $MgFe_2O_4$, $KCrO_2$	$MgSiO_4$, SiO_2	0.022
	-	347	$MgFe_2O_4$, Fe_3O_4, Fe_2O_3	Na_2O	0.021
Solar Salt ISS Grade	Al_2O_3 (1 wt%)	347	$MgFe_2O_4$, $MgAl_2O_4$, Fe_2O_3	Fe_3O_4, Al_2O_3, $Ca_2Fe_2O_5$	0.019
	SiO_2 (1 wt%)	347	$MgFe_2O_4$, Fe_3O_4, MgO, SiO_2, Fe_2SiO_4	SiO_2, $Ca_2Fe_2O_5$	0.024
	-	347	$MgFe_2O_4$, Fe_3O_4, MgO, $MgCr_2O_4$	Fe_2O_3, $MgFe_2O_4$	0.027

341

342 The gravimetric corrosion rate was also included in the table 2. ISS mixture showed the
343 higher corrosion rate due to the higher Cl content. The effect of nanoparticles does not
344 seem to increase the corrosion rate obtained in the isothermal static study at 565ºC. It has
345 been found that Al_2O_3 nanoparticles present a better corrosion protection of the steel
346 matrix when using RSS salts rather than using ISS salts. This effect could be interesting
347 in order to design a protective methodology for the steels in contact with the salt since a
348 superficial Al content has been detected. On the other hand, this corrosion-protective
349 layer formed onto the steel reduces the content of the Al_2O_3 nanoparticles in the salt,
350 whose main function is the enhancement of the thermal properties. Corrosion rates are in
351 concordance with the results available in literature, regarding the immersion of 347SS in
352 RSS. Kruizenga [21] reported a weight loss around 1.8 mg/cm^2 in same conditions at
353 1000 hours of test, which correspond to a corrosion rate of 0.02 mm/year.

354

355

4. Conclusions

The present work has carried out a corrosion study of a commercial stainless steel (347SS) into nanofluids made of solar salt doped with 1%wt. of nanoparticles. The study comprises tests with two different grades of solar salt (refined and industrial) and two different types of nanoparticles, Silica and Alumina.

The results obtained in the corrosion study showed a higher corrosion rate using the industrial solar salt grade, due to the higher chloride content, compared with the other impurity grade (RSS) but the addition of nanoparticles do not increase the corrosion behavior in the storage materials tested.

According with the results obtained, for RSS + 1wt% Al_2O_3, a protective layer was obtained. This structure (composed mainly by Al_2O_3) and integrated in the steel matrix, increase the protection against the corrosion produced by molten salts.

One of the drawbacks detected in the nanofluid was a reduction of the viscosity in the salt during the corrosion test, when SiO_2 nanoparticles are involved. In this case, solidification of the salt was produced during the test and the XRD analysis revealed the presence of SiO_2 and $MgSiO_4$, as main component in the salt remaining after the corrosion test.

The corrosive evaluation of these nanofluid showed that nanoparticles do not produce an enhancement of the corrosion rate in static conditions. However, the corrosion should also be tested in dynamic conditions since Al_2O_3/SiO_2 are solid particles in the mixture, being potential candidates to promote erosion/corrosion in CSP pipelines.

Acknowledgement

The authors would like to acknowledge the financial support provided by CONICYT / FONDAP 15110019 "Solar Energy Research Center" SERC-Chile. The authors wish to acknowledge the University of the Basque Country UPV/EHU for supporting the PhD of Belén Muñoz-Sánchez (Zabalduz program) and her research stay at the Universidad de Antofagasta.

References

1. D. Kearney, B.K., R. Mahoney *Assessment of a molten heat transfer fluid in a parabolic trough solar field.* Solar Energy Engineering, 2002.
2. Fernandez, A. G., S. Ushak, H. Galleguillos, F.J Perez "Development of new molten salts with LiNO3 and Ca(NO3)2 for energy storage in CSP plants." Applied Energy, 2014, 119: 131-140.
3. Fernandez, A.G., Vidal-Gomez J., *Thermophysical properties of low cost lithium nitrate salts produced in northern Chile for thermal energy storage.* Renewable Energy, 2016. 101: p. 120-125.
4. Jo, Byeongnam and D. Banerjee, *Enhanced specific heat capacity of molten salt-based nanomaterials: Effects of nanoparticle dispersion and solvent material.* Acta Materialia, 2014, 75: p. 80-91.
5. Muñoz-Sanchez, B., J. Nieto-Maestre, I. Iparraguirre-Torres, A. García-Romero, J.M. Sala-Lizarraga, *Molten salt-based nanofluids as efficient heat transfer and storage materials at high temperatures. An overview of the literature.* Renewable and Sustainable Energy Reviews. 2017, 82: p. 3924-3945.
6. Ho, M.X. and C. Pan, *Optimal concentration of alumina nanoparticles in molten Hitec salt to maximize its specific heat capacity.* International Journal of Heat and Mass Transfer, 2014, 70(0): p. 174-184.
7. Ho, M.X. and C. Pan, *Experimental investigation of heat transfer performance of molten HITEC salt flow with alumina nanoparticles.* International Journal of Heat and Mass Transfer, 2017, 107: p. 1094-1103.
8. Alashkar, A. and M. Gadalla, *Thermo-economic analysis of an integrated solar power generation system using nanofluids.* Applied Energy, 2017, 191: p. 469-491.
9. Madathil, P.K., *Preparation and characterization of molten salt based nanothermic fluids with enhanced thermal properties for solar thermal applications.* Applied Thermal Engineering, 2016, 109: p. 901-905.
10. Tian, H., *Enhanced Specific Heat of Chloride Salt with Mg Particles for High-temperature Thermal Energy Storage.* Energy Procedia, 2017, 105: p. 4402-4407.
11. D. Shin, D.B., *Enhanced specific heat of silica nanofluid.* J. Heat Transfer, 2011. 133: p. 024501.
12. D. Shin, D.B., *Enhanced specific heat capacity of nanomaterials synthesized by dispersing silica nanoparticles in eutectic mixtures.* J. Heat Transfer 2013. 135: p. 032801.
13. Gasia, J., L. Miro, and L.F. Cabeza, *Review on system and materials requirements for high temperature thermal energy storage. Part 1: General requirements.* Renewable and Sustainable Energy Reviews, 2017, 75: p. 1320-1338.
14. Kruizenga, A.M., *Corrosion Mechanisms in Chloride and Carbonate Salts.* Sandia Report, 2012. SAND2012-7594.
15. Fernandez, A.G., M. Grageda, and H. Galleguillos, *Impurity Influence in Physico-chemical and Corrosion Properties of Chilean Solar Nitrates.* Energy Procedia, 2014, 49: p. 607-616.
16. Fernandez, A.G., H. Galleguillos, and F.J. Perez, *Thermal influence in corrosion properties of Chilean solar nitrates.* Solar Energy, 2014, 109(0): p. 125-134.
17. Groll, M., O. Brost, and D. Heine, *Corrosion of steels in contact with salt eutectics as latent heat storage materials: Influence of water and other impurities.* Heat Recovery Systems and CHP, 1990. 10(5-6): p. 567-572.

18. Muñoz-Sanchez, B., J. Nieto-Maestre, *A precise method to measure the specific heat of solar salt-based nanofluids.* Journal of Thermal Analysis and Calorimetry, 2017. 192(2): p. 905-914.
19. Abdel Hamid, Z., S. Abd El Rehim, *Effectiveness of Si contents in the steel composition on the corrosion performance of galvanized steel.* Anti-Corrosion Methods and Materials, 2017. 65(5): p. 479-485.
20. Yang, C., *NOx emissions and the component changes of ternary molten nitrate salts in thermal energy storage process.* Applied Energy, 2016, 184: p. 346-352.
21. A.M. Kruizenga, D.D.G., M. LaFord, *Materials Corrosion of High Temperature Alloys Immersed in 600 °C Binary Nitrate Salt.* SAND2013-2526., 2013.

Highlights:

- Corrosion rates obtained during the experiments are similar using nanosalts or conventional nitrate molten salts.
- The knowledge acquired in corrosion using nanosalts can help to understand the corrosion issues associated with doped molten salts under operation in CSP plants.
- The use of molten salts doped with Al_2O_3 nanoparticles could increase the corrosion resistance in steels in contact with them